Donor-Acceptor-Acceptor' Molecules for Vacuum-deposited Organic Photovoltaics with Efficiency Exceeding 9%

Xiaozhou Che[#], Chin-Lung Chung[#], Chou-Chun Hsu, Feng Liu, Ken-Tsung Wong[*], and Stephen R. Forrest[*]

# These authors contributed equally.

X. Che, Prof. S. R. Forrest
Applied Physics Program
University of Michigan
Ann Arbor, MI 48109, USA
E-mail: stevefor@umich.edu

C.-L. Chung, C.-C. Hsu, Prof. K.-T. Wong
Department of Chemistry
National Taiwan University
Taipei, 10617, Taiwan
E-mail: kenwong@ntu.edu.tw

F. Liu
Department of Physics and Astronomy, and Collaborative Innovation Center of IFSA (CICIFSA)
Shanghai Jiaotong University,
Shanghai 200240, P. R. China.

Prof. K.-T. Wong
Institute of Atomic and Molecular Science, Academia Sinica
Taipei, 10617, Taiwan

Prof. S. R. Forrest
Departments of Physics, and Department of Electrical Engineering and Computer Science
University of Michigan
Ann Arbor, MI 48109, USA

Abstract

We study three vacuum-deposited donor-acceptor-acceptor' (d-a-a') small molecule donors with different side chains attached to an asymmetric heterotetracene donor block for use in high efficiency organic photovoltaics (OPVs). The donor with an isobutyl side chain yields the highest crystal packing density compared to molecules with 2-ethylhexyl or *n*-butyl chains, leading to the largest absorption coefficient and short circuit current in an OPV. It also exhibits a higher fill factor, consistent with its preferred out-of-plane molecular π-π stacking arrangement that facilitates charge transport in the direction perpendicular to the substrate. A power conversion efficiency of 9.3 ± 0.5% is achieved under 1 sun intensity, AM 1.5G simulated solar illumination, which is significantly higher than 7.5 ± 0.4% of the other two molecules. These results indicate that side chain modification of d-a-a' small molecules offers an effective approach to control the crystal packing configuration, thereby improving the device performance.

Organic photovoltaics (OPVs) are emerging as a means for providing renewable energy at low cost and with low environmental impact.[1, 2] A class of vacuum-deposited, donor-acceptor-acceptor' (d-a-a') small molecule donors have been introduced to increase the efficiency of OPVs fabricated via vacuum thermal evaporation (VTE).[3-5] These materials consist of an electron-donating (d) unit attached to two connected electron-accepting (a, a') groups. The rod-like molecular backbones with strong push-pull interactions between the 'd' and 'a' units result in a large ground state dipole moment that induce ordered π-π stacking and favors intermolecular charge transfer.[6, 7] Further, the d-a-a' motif allows for adjustment of molecular conjugation using different functional groups. Recently we described the effects of cross-conjugation of d-a-a' small molecule donors on the open circuit voltages (V_{OC}) of fullerene-based OPVs. A linear correlation was established between the reciprocal of

molecular conjugation length, the highest occupied molecular orbital (HOMO) energy, and V_{OC}.[5] Among the d-a-a' donors studied, 2-((7-(N-(2-ethylhexyl)-benzothieno[3,2-b]thieno[2,3-d]pyrrol-2-yl)benzo[c][1,2,5]thiadiazol-4-yl)methylene)malononitrile (antiBTDC, Fig. 1a) comprising a benzothiadiazole-dicyanovinylene a-a' unit coupled to an asymmetric heterotetracene donor block achieved power conversion efficiency of $PCE = 7.2 \pm 0.3\%$.

Modification of the side chain length also serves as an effective approach to optimize small molecule performance. For example, Bäuerle *et al.* altered the side chains linked to the donor moiety of a-d-a-configured molecules with propyl, hexyl and *p*-tolyl groups.[8] The changes induced in morphology led to an increase in *PCE* from 3.7% to 5.6% as the alkyl chain lengths decreased (hexyl vs. propyl). Moreover, it has been reported that subtle variations of molecular alkyl substitutions affects the tendency for crystallization.[9] Yet, molecules with shortened side chains are difficult to purify by column chromatography because of their insufficient solubility in common organic solvents. Therefore, there is a trade-off between desired material properties and processability.

In this work, we synthesized and characterized two d-a-a' small molecules to analyze the effects of side chains on device performance. The molecules shown in Fig. 1b and 1c are 2-((7-(N-(isobutyl)-benzothieno[3,2-*b*]thieno[2,3-*d*]-pyrrol-2-yl)benzo[*c*][1,2,5]thiadiazol-4-yl)methylene)malononitrile (iBuBTDC) and 2-((7-(N-(n-butyl)-benzothieno[3,2-*b*]thieno[2,3-*d*]-pyrrol-2-yl)benzo[*c*][1,2,5]thiadiazol-4-yl)methylene) malononitrile (nBuBTDC). They share the same backbone structure as antiBTDC, while iBuBTDC possesses a shorter branched isobutyl chain and nBuBTDC has an *n*-butyl chain. The alkyl chains of iBuBTDC and nBuBTDC are smaller than antiBTDC but still provide sufficient solubility during column chromatography purification. The OPVs based on iBuBTDC mixed

with C_{70} yields the largest short circuit current (J_{SC}), which is consistent with the largest absorption coefficient among the three molecules. In addition, the preferred out-of-plane stacking arrangement of iBuBTDC facilitates charge transfer perpendicular to the substrate, thereby increasing the fill factor (*FF*). The iBuBTDC:C_{70} cell achieves *PCE* = 9.3 ± 0.5% under 1 sun intensity (100 mW/cm^2), AM 1.5G simulated solar illumination, with J_{SC} = 16.5 ± 0.8 mA/cm^2, open circuit voltage V_{OC} = 0.94 ± 0.01V and *FF* = 0.60 ± 0.01. Solar cells employing nBuBTDC, on the other hand, shows a trade-off between the low *FF* and high J_{SC}, giving *PCE* = 7.5 ± 0.4% which is comparable to that of antiBTDC. These results indicate that proper selection of the side chain incorporated into d-a-a' molecules provides a route to enhanced crystal packing, while maintaining a sufficient solubility for synthesis and purification.

The different lengths and shapes of the side chains of antiBTDC, iBuBTDC and nBuBTDC shown in Fig. 1 (indicated by red circles) result in different molecular conformations between the central thiophene and the benzothiadiazole acceptor units along the intervening C–C single bond that connects them. The antiBTDC exhibits a *s*-trans arrangement (Fig. 1a, blue circles), while iBuBTDC and nBuBTDC are *s*-cis conformation (Fig. 1b and 1c). The electronic transition parameters computed from density functional theory (DFT) are listed in Table S1 in Supporting Information. The three donors possess similar HOMO - lowest unoccupied molecular orbital (LUMO) energies, and lowest energy singlet ground-to-excited state transition ($S_1 \leftarrow S_0$) molecular orbital (MO) compositions (98% HOMO→LUMO, plus 2% HOMO-1→LUMO). The oscillator strengths (*f*) of the $S_1 \leftarrow S_0$ transition are also similar, with $f \sim 1.1$.

The antiparallel arrangement of centrosymmetric dimer stacks is observed in crystals of all three molecules due to the large ground state dipole moment of > 10 D. Figure 2 shows

the packing configurations of the donor molecules with structural parameters summarized in Table 1. The molecules with different side chains show similar average intermolecular π-π distances of between 3.44 to 3.49 Å. A dihedral angle of 8.8° between the thienoacene donor and benzothiadiazole acceptor is observed in antiBTDC, while both iBuBTDC and nBuBTDC present almost perfect coplanar conformations with dihedral angles of 3.4° and 2.0°, respectively. The longer alkyl chain of antiBTDC separates the adjacent π-π stacks with a distance of 12.3 Å (Fig. 2a), while iBuBTDC tends to pack more compactly, with a distance of 6.1 Å between adjacent stacks (Fig. 2b). The nBuBTDC, however, forms orthogonal stacks, as shown in Fig. 2c. The packing densities of iBuBTDC and nBuBTDC are 1.496 g/cm^3 and 1.469 g/cm^3, respectively, which is considerably higher than that of antiBTDC (1.407 g/cm^3).

Cyclic voltammograms (CV) of iBuBTDC and nBuBTDC are shown in Fig. S1. Data for antiBTDC are published elsewhere.[5] The HOMO and LUMO energies for both iBuBTDC and nBuBTDC based on the oxidation potential and the first reduction potential are -5.35 eV and -3.83 eV, respectively. Figure 3a presents the absorption coefficients of the donor films. The molecules all show absorption between wavelengths of λ = 450 and 800 nm, with a peak at λ = 620 nm. This is consistent with the energy gap of 1.52 eV measured by CV (Table S2). The absorption coefficient of iBuBTDC is slightly larger than nBuBTDC, both of which are about 20% higher than antiBTDC (Fig, 3a), which can be attributed to the higher packing density of the former molecules. In addition, all the molecules have thermal decomposition temperatures (T_d, corresponding to 5% weight loss) of 340-350 ^{o}C measured by thermogravimetric analysis. The detailed photophysical and electrochemical parameters of the molecules are summarized in Table S2.

The external quantum efficiency (*EQE*) and current density-voltage (*J-V*) characteristics of the three d-a-a' OPV devices with 1:3 donor:acceptor (D:A) ratio and 70 nm active layer are compared in Fig. 3b and 3c (solid lines), with details summarized in Table 2 (see Experimental Section and Fig. S2 for structures and optimization). All three cells exhibit photoresponse between wavelengths of λ = 350 to 800 nm, with V_{OC} > 0.9 V. The iBuBTDC (red circle) cell shows the highest response in the NIR region with *EQE* ~ 65% at 650 nm. The J_{SC} of iBuBTDC:C_{70} and nBuBTDC:C_{70} are 16.1 ± 0.8 mA/cm^2 and 15.7 ± 0.8 mA/cm^2, respectively, compared to 14.4 ± 0.7 mA/cm^2 for antiBTDC:C_{70}. With a higher J_{SC} but lower *FF* than antiBTDC:C_{70}, the nBuBTDC:C_{70} gives a similar *PCE* = 7.5 ± 0.4% at 1 sun, AM 1.5G illumination. On the other hand, the iBuBTDC device achieves *FF* = 0.58 ± 0.01 and *PCE* = 8.8 ± 0.5%, the highest among the three donors. Further improvement of the iBuBTDC device performance is achieved by additional purification of the source material using temperature-gradient sublimation[10], resulting in an increase in *FF* from 0.58 ± 0.01 to 0.60 ± 0.01. The iBuBTDC:C_{70} cell with 80 nm thick active layer grown from the purified iBuBTDC achieves *PCE* = 9.3 ± 0.5%, with J_{SC} = 16.5 ± 0.8 mA/cm^2, V_{OC} = 0.94 ± 0.01 V and *FF* = 0.60 ± 0.01. The *EQE* and *J-V* characteristics of this iBuBTDC:C_{70} cell are plotted as dashed lines in Figs. 3b and 3c. Atomic force microscopy (AFM) images of the mixed active layers are shown in Fig. S3. They present similar surface morphologies with mean square roughnesses of 0.35-0.40 nm.

To further understand the effects of side chains on morphology and device performance, grazing incidence x-ray diffraction (GIXD)[11] was performed on vacuum-deposited films grown on Si substrates pre-coated with a 10 nm thick layer of MoO₃. Shown in Fig. 4a and 4b are the diffraction patterns and the corresponding line-cut profiles of the neat donor and acceptor samples. The iBuBTDC film shows a (100) diffraction peak in the

out-of-plane (q_z) direction at 0.61 Å^{-1}, with a crystal coherence length of CCL_z = 2.5 nm. The π-π stacking is seen in both in-plane (q_{xy}) and q_z directions with a full azimuthal angular spreading at 1.79 Å^{-1}, corresponding to a distance of 0.35 nm, and CCL_{xy} = 2.1 nm. The nBuBTDC molecule shows a similar morphology with the (100) diffraction peak at q_z = 0.58 Å^{-1} (CCL_z = 2.8 nm) and π-π stacking at 1.78 Å^{-1} (CCL_{xy} = 2.7 nm). The antiBTDC exhibits longer range order with a (100) peak at q_z = 0.49 Å^{-1} (CCL_z = 4.0 nm); and a π-π peak at q_{xy} = 1.79 Å^{-1} (CCL_{xy} = 2.7 nm). The C_{70} acceptor thin film also shows molecular packing with the (100) diffraction at q_z = 0.72 Å^{-1}, with CCL_z = 8.5 nm, and the (010) and (001) diffraction peaks at 1.21 Å^{-1} and 1.39 Å^{-1} respectively. A weak diffraction ring is seen at 1.86 Å^{-1}, corresponding to a distance of 0.34 nm characteristic of the C_{70} intermolecular spacing. The GIXD patterns of d-a-a':C_{70} blend films were also obtained and shown in Fig. S4. However, the diffraction patterns are dominated by the C_{70} component due to its improved crystallinity over that of the d-a-a' donors, preventing differentiation between the morphologies of the three blends.

The foregoing results lead to the conclusion that the d-a-a' molecules with different side chain configurations lead to different optical and electrical properties in their thin films. The smaller isobutyl and n-butyl chains attached to the backbones of iBuBTDC and nBuBTDC, respectively, provide less steric hindrance then the 2-ethylhexyl chain of antiBTDC, resulting in smaller dihedral angles between the benzothiadiazole acceptor group and the thienoacene donor unit. The same calculated oscillator strength associated with the $S_1 \neg S_0$ transition of the three donor molecules, however, indicates a similar degree of molecular orbital overlap. This confirms that the side chains do not have a direct impact on the electronic coupling between the donor and acceptor units along the molecular backbone, and thus on the intramolecular charge transfer. The cyclic voltammograms of iBuBTDC and

7

nBuBTDC are similar to that of antiBTDC, suggesting that the electrochemical properties are also not significantly affected by the side chains. The differences in absorption coefficient as well as device performance, therefore, are more closely related to intermolecular charge transfer and the packing morphologies.

Dipolar d-a-a' molecules tend to form dimer units that are packed in a slipped-stack manner. All three donors form long-range π-stacked networks as shown in Fig. 2. The closer crystal packing distance between iBuBTDC molecules due to its shorter isobutyl side chain (Fig. 2b) leads to a higher absorption coefficient and J_{SC} than the other two molecules studied, followed by the nBuBTDC with slightly lower packing density. The relatively long, branched side chain of antiBTDC leads to the lowest density, therefore the smallest J_{SC}. As seen in Fig. 3b, all three devices exhibit nearly wavelength-independent EQE across the visible spectrum due to the balanced absorption of the optimized 1:3 D:A active region blends.

An important factor that differentiates the performance of devices based on the three compounds are their FFs due to differences in their in-plane and out-of-plane stacking motifs shown in Fig. 4a. The strongest diffraction signal in the in-plane direction with almost no out-of-plane component is observed for antiBTDC, suggesting a preferred edge-on orientation. In contrast, iBuBTDC shows the most intense signal along q_z, while nBuBTDC shows diffraction intermediate between the two molecules. The higher ratio of face-on π-π stacking in the iBuBTDC film leads to efficient charge transport perpendicular to the substrate, resulting in the highest FF. As seen in Fig. S2d, FF and V_{OC} of the iBuBTDC:C$_{70}$ are relatively independent of active layer thickness up to 80 nm, indicating significant long-range order. A 10% relative improvement of FF is observed for the iBuBTDC:C$_{70}$ cell compared

with nBuBTDC:C_{70}, which is likely due to the orthogonal arrangement between the adjacent stacks of nBuBTDC molecules that impedes intermolecular charge transfer.

In summary, we analyzed the effects of side chain length and shape of small molecule d-a-a' donors on vacuum-deposited thin film properties and OPV performance. Two new donors (iBuBTDC and nBuBTDC) modified from the previously reported antiBTDC are synthesized, featuring shorter branched and straight alkyl chains, respectively. The various side chains attached to the same d-a-a' backbone show the same π-π stacking distance of ~3.5 Å but different crystal packing configurations, resulting in distinct absorption and charge transfer properties of the three donor molecules. The iBuBTDC with its short isobutyl chain forms a compact arrangement between adjacent π-π stacks that leads to the highest film density. Based on GIXD measurements, iBuBTDC also shows the largest out-of-plan π-π stacking diffraction intensity, while antiBTDC stacks mostly in the in-plane direction. The iBuBTDC therefore achieves improved absorption and intermolecular charge transport compared with antiBTDC, leading to higher OPV J_{SC} and *FF* with the highest *PCE* = 9.3 ± 0.5%. The nBuBTDC with n-butyl side chain has a similar absorption coefficient and J_{SC} to iBuBTDC. However, the orthogonal packing arrangement between neighbor stacks hinders intermolecular charge transfer that significantly reduces the *FF*, giving a *PCE* = 7.5 ± 0.4%, similar to that of antiBTDC. These results suggest that the side chains of d-a-a' small molecule donors play an important role in crystal packing that provides an opportunity to fine tune morphology to achieve a significantly improved device performance.

Experimental Section

The d-a-a' donor molecules (antiBTDC, iBuBTDC and nBuBTDC) with different side chain configurations were synthesized at the National Taiwan University, with the details reported in Supporting Information Scheme S1. Other materials were purchased from commercial vendors: MoO_3 (Acros Organics), BPhen (Luminescence Technology Corp.), C_{60} (MER), C_{70} (SES Research) and Ag (Alfa Aesar). The d-a-a' donors were purified by column chromotagraphy. The C_{60}, C_{70} and one batch of iBuBTDC went through temperature-gradient sublimation purification prior to use.

The absorption coefficients of the neat donors were measured by UV-VIS (Perkin Elmer 1050). Cyclic voltammetry (CH Instruments, Inc. CH1619B) was measured by a three-electrode electrochemical cell with a glassy carbon working electrode, a Pt wire counter electrode, and a Ag/AgCl reference electrode.

Organic solar cells were grown on pre-patterned indium tin oxide (ITO)-glass substrates with a sheet resistance ~15 Ω/sq (purchased from Lumtec). Immediately prior to growth, the substrates were cleaned in a series of detergents and solvents and exposed to ultraviolet-ozone for 10 min that modifies the ITO work function for better ohmic contact with MoO_3. The layers were deposited by vacuum thermal evaporation in a chamber with a base pressure of 10^{-7} torr attached to a glove box filled with ultrapure N_2 (O_2, H_2O < 0.1 ppm) for sample loading and storage. Organic layers and metals were deposited through different shadow masks attached directly to the substrate. All the layers were deposited or co-deposited at the rate of 0.1 nm/s. For blend films, the rate of each component was adjusted to achieve the desired volume ratios. Quartz crystal monitors placed in the chamber were used to monitor the deposition rates and thicknesses, calibrated by variable-angle spectroscopic ellipsometry.

Devices are fabricated with the structure: indium tin oxide (ITO)/MoO$_3$ (10 nm)/d-a-a' donor:C$_{70}$/bathophenanthroline (BPhen):C$_{60}$ (1:1 ratio by vol., 10 nm)/ BPhen (5 nm)/Ag (100 nm). The transparent and conductive MoO$_3$ is used as the anode buffer[12], while the mixed buffer consisting of a BPhen:C$_{60}$ (1:1) layer capped with a neat BPhen layer is inserted between the active layer and the cathode for efficient electron conduction and exciton blocking[13]. The donor:acceptor (D:A) ratio and thickness was optimized to achieve the highest OPV efficiency. The optimization of iBuBTDC:C$_{70}$ cell is taken as an example in Fig. S2. All OPVs show the best performance with a D:A ratio of 1:3 and active layer thicknesses between 70 nm and 80 nm. The device area of 2 mm^2 is defined by the overlap between the patterned ITO anode and the Ag cathode.

The devices were measured in a glovebox with ultrapure N$_2$ environment. The current density-voltage (J-V) characteristics were obtained using a filtered Xe solar simulator with AM 1.5G illumination spectrum (ASTM G173-03). The lamp intensity was calibrated by a National Renewable Energy Laboratory (NREL) traceable Si reference cell, and adjusted with neutral density filters. For external quantum efficiency (EQE) measurement, the devices as well as a reference NIST-traceable calibrated Si photodetector were underfilled with a focused beam of monochromated light from a Xe-lamp chopped at 200 Hz. The generated current was input to a lock-in amplifier to record the photo response at each wavelength. The J_{SC} values reported in Table 2 are determined from the integrated EQE spectra, which are within $\pm$ 3% compared with the J_{SC} from the J-V measurement. The error bars quoted in the table take into account of both the measurement and systematic errors.

The grazing incidence x-ray diffraction (GIXD) data were collected at Lawrence Berkeley National Lab (LBNL), with beamline 7.3.3 at the Advanced Light Source (ALS). The X-ray with 10 keV energy was operated in the top-off mode, while a 2D image plate

(Pilatus 1M) with a pixel size of 172 μm (981 × 1043 pixels) was used to record the scattered signal. The sample and the detector were separated by 30 cm along the beam path. The incidence angle was chosen to be 0.16° that is above the critical angle.

References

[1]   S. E. Shaheen, D. S. Ginley, G. E. Jabbour, *MRS Bull.* **2011**, *30*, 10.

[2]   S. B. Darling, F. You, *RSC Advances* **2013**, *3*, 17633.

[3]   Y.-H. Chen, L.-Y. Lin, C.-W. Lu, F. Lin, Z.-Y. Huang, H.-W. Lin, P.-H. Wang, Y.-H. Liu, K.-T. Wong, J. Wen, D. J. Miller, S. B. Darling, *J. Am. Chem. Soc.* **2012**, *134*, 13616.

[4]   L.-Y. Lin, Y.-H. Chen, Z.-Y. Huang, H.-W. Lin, S.-H. Chou, F. Lin, C.-W. Chen, Y.-H. Liu, K.-T. Wong, *J. Am. Chem. Soc.* **2011**, *133*, 15822.

[5]   X. Che, C.-L. Chung, X. Liu, S.-H. Chou, Y.-H. Liu, K.-T. Wong, S. R. Forrest, *Adv. Mater.* **2016**, *28*, 8248.

[6]   H. Bürckstümmer, E. V. Tulyakova, M. Deppisch, M. R. Lenze, N. M. Kronenberg, M. Gsänger, M. Stolte, K. Meerholz, F. Würthner, *Angew. Chem.* **2011**, *123*, 11832.

[7]   O. L. Griffith, X. Liu, J. A. Amonoo, P. I. Djurovich, M. E. Thompson, P. F. Green, S. R. Forrest, *Phys. Rev. B* **2015**, *92*, 085404.

[8]   A. Mishra, D. Popovic, A. Vogt, H. Kast, T. Leitner, K. Walzer, M. Pfeiffer, E. Mena-Osteritz, P. Bäuerle, *Adv. Mater.* **2014**, *26*, 7217.

[9]   J. Liu, Y. Sun, P. Moonsin, M. Kuik, C. M. Proctor, J. Lin, B. B. Hsu, V. Promarak, A. J. Heeger, T.-Q. Nguyen, *Adv. Mater.* **2013**, *25*, 5898.

[10]   S. R. Forrest, *Chem. Rev.* **1997**, *97*, 1793.

[11]   S. E. Fritz, S. M. Martin, C. D. Frisbie, M. D. Ward, M. F. Toney, *J. Am. Chem. Soc.* **2004**, *126*, 4084.

[12]   N. Li, B. E. Lassiter, R. R. Lunt, G. Wei, S. R. Forrest, *Appl. Phys. Lett.* **2009**, *94*, 023307.

[13]   A. N. Bartynski, C. Trinh, A. Panda, K. Bergemann, B. E. Lassiter, J. D. Zimmerman, S. R. Forrest, M. E. Thompson, *Nano Lett.* **2013**, *13*, 3315.

Table 1. Crystal packing parameters of antiBTDC, iBuBTDC and nBuBTDC.

Crystal parameter	antiBTDC	iBuBTDC	nBuBTDC
Crystal system	Triclinic	Triclinic	Monoclinic
Dihedral angle (^{o})	8.8	3.4	2.0
Average intermolecular π-π distance (Å)	3.47	3.44	3.49
Packing density (g/cm^3)	1.407	1.496	1.469

Table 2. Performance of the d-a-a' donor:C_{70} OPV cells.

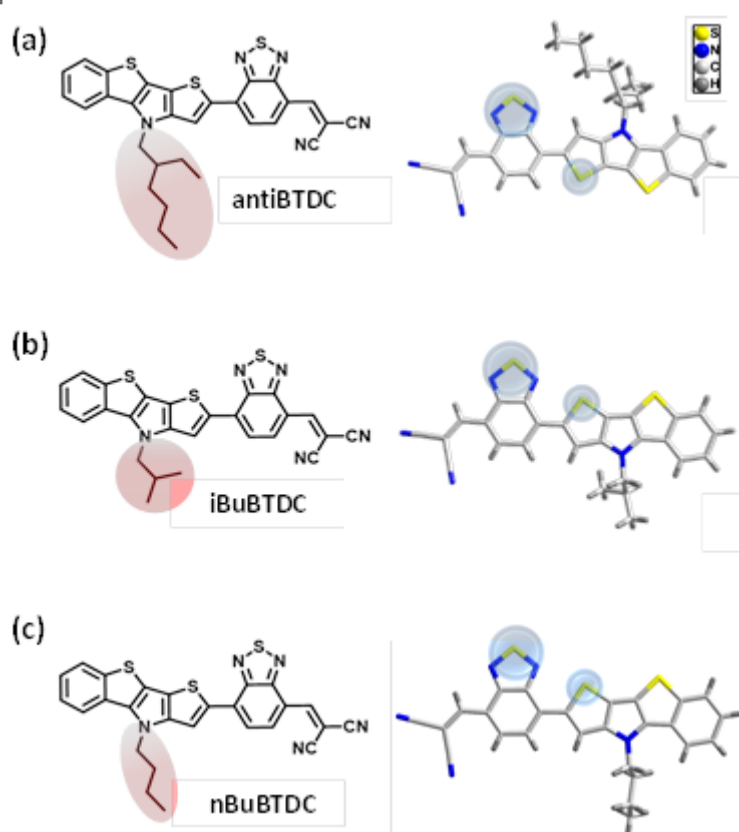| Device	J_{SC} (mA/cm^2)	V_{OC} (V)	FF	PCE (%)
iBuBTDC:C_{70}	16.1 ± 0.8	0.94 ± 0.01	0.58 ± 0.01	8.8 ± 0.5
	16.5 ± 0.8	0.94 ± 0.01	0.60 ± 0.01	9.3 ± 0.5*
nBuBTDC:C_{70}	15.7 ± 0.7	0.92 ± 0.01	0.52 ± 0.01	7.5 ± 0.4
antiBTDC:C_{70}	14.4 ± 0.7	0.93 ± 0.01	0.56 ± 0.01	7.5 ± 0.4

*iBuBTDC with additional temperature-gradient sublimation.

Figure 1. (left) Molecular structural formulae and (right) atomic arrangements of a) antiBTDC, b) iBuBTDC and c) nBuBTDC.
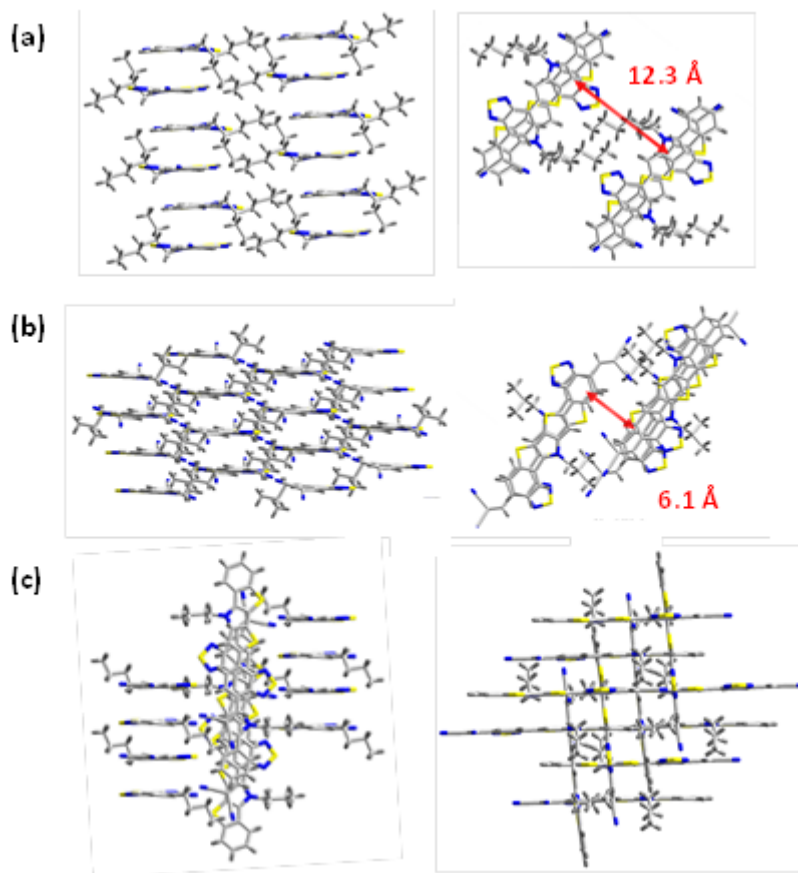
Figure 2. Crystal packing configurations of a) antiBTDC, b) iBuBTDC and c) nBuBTDC. The intermolecular interplanar spacings of antiBTDC and iBuBTDC are indicated by the red arrows.
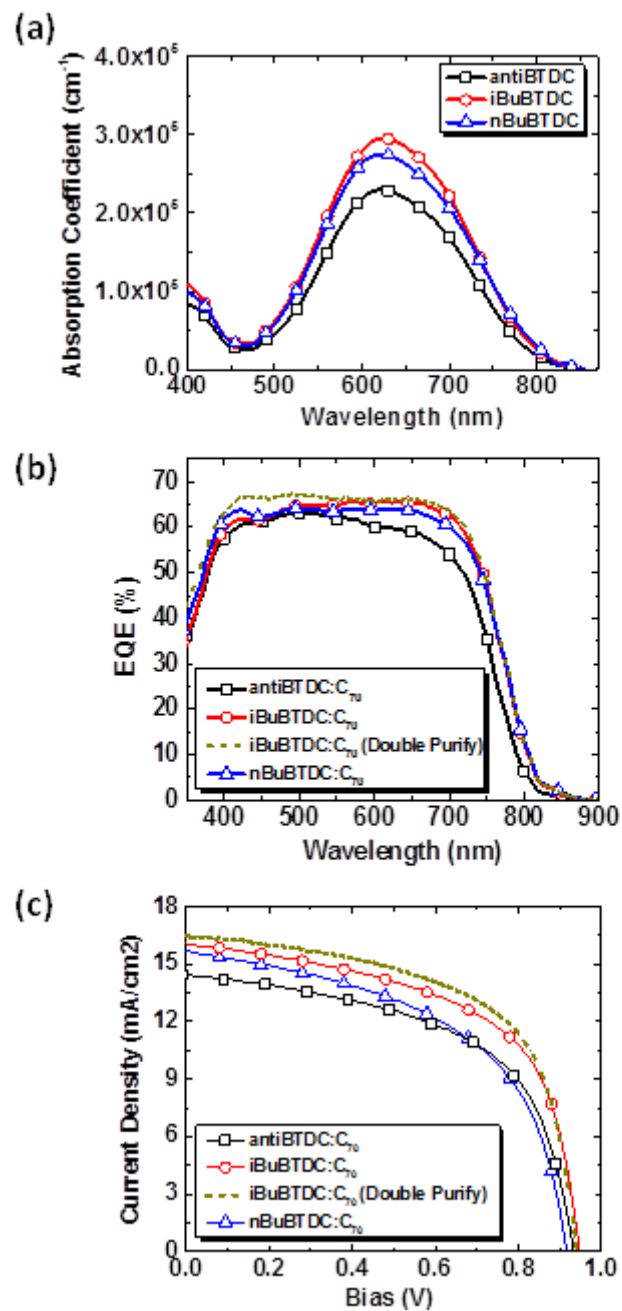
Figure 3. a) Absorption coefficients vs. wavelength of the neat d-a-a' donors in solid state. b) External quantum efficiency (*EQE*) and c) current density-voltage (*J-V*) characteristics of the optimized d-a-a':C_{70} cells for the various donors studied.
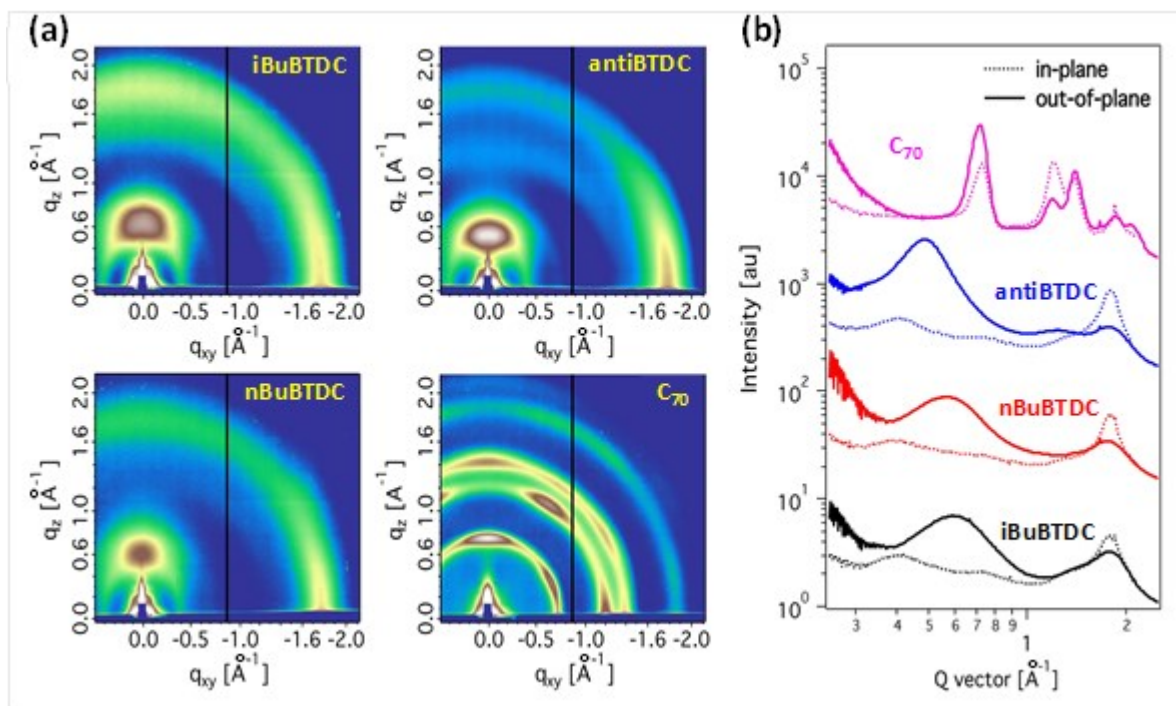
Figure 4. a) Two-dimensional grazing incidence X-ray diffraction (GIXD) scattering patterns of vacuum deposited donor and acceptor thin films; and b) the corresponding line cut profiles.

Three vacuum-deposited donor-acceptor-acceptor' small molecule donors with different alkyl chain configurations (R_1-R_3) are synthesized and characterized to understand the side chain effect on organic photovoltaic (OPV) performance. The donor with an isobutyl (R_3) chain yields the highest crystal packing density and largest short circuit current among the three molecules. Its preferred face-on molecular stacking orientation on the substrate leads to the highest fill factor. The optimized OPV structure achieves power conversion efficiency (*PCE*) = 9.3 ± 0.5%.